Single Molecule Force Measurements in Living Cells Reveal a Minimally Tensioned Integrin State

Alice C. Chang[1], **Armen H. Mekhdjian**[1], **Masatoshi Morimatsu**[2], **Aleksandra K. Denisin**[3,4], **Beth L. Pruitt**[4,5,6], and **Alexander R. Dunn**[1,5,*]

[1]Department of Chemical Engineering, Stanford University, Stanford, California 94305, United States

[2]Graduate School of Medicine, Dentistry, and Pharmaceutical Sciences, Okayama University, Okayama, Japan

[3]Department of Bioengineering, Stanford University, Stanford, California 94305, United States

[4]Department of Mechanical Engineering, Stanford University, Stanford, California 94305, United States

[5]Stanford Cardiovascular Institute, Stanford University, 265 Campus Drive Stanford, California 94305, United States

[6]Department of Molecular and Cellular Physiology, Stanford University School of Medicine, Stanford, California 94305, United States

Abstract

Integrins mediate cell adhesion to the extracellular matrix and enable the construction of complex, multicellular organisms, yet fundamental aspects of integrin-based adhesion remain poorly understood. Notably, the magnitude of the mechanical load experienced by individual integrins within living cells is unclear, due principally to limitations inherent to existing techniques. Here we use FRET-based molecular tension sensors (MTSs) to directly measure the distribution of loads experienced by individual integrins in living cells. We find that a large fraction of integrins bear modest loads of 1–3 pN, while subpopulations bearing higher loads are enriched within adhesions. Further, our data indicate that integrin engagement with the fibronectin synergy site, a secondary binding site specifically for $\alpha_5\beta_1$ integrin, leads to increased levels of $\alpha_5\beta_1$ integrin recruitment to adhesions but not to an increase in overall cellular traction generation. The presence of the synergy site does, however, increase cells' resistance to detachment by externally applied loads. We suggest that a substantial population of integrins experiencing loads well below their peak capacities can provide cells and tissues with mechanical integrity in the presence of widely varying mechanical loads.

Graphical Abstract

---

*alex.dunn@stanford.edu.
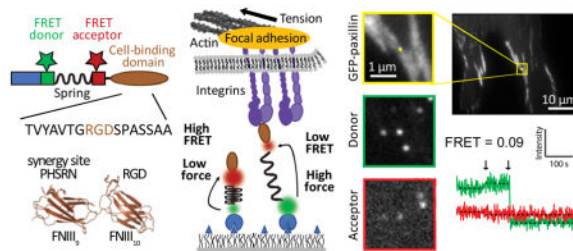
Keywords

integrin; cell adhesion; mechanobiology; single molecule; tension sensor

Integrins are heterodimeric transmembrane proteins that link the extracellular matrix (ECM) to the cell cytoskeleton and critically influence cell migration, proliferation, and differentiation. Integrins are composed of an α and β subunit, of which 18 and 8 have been identified in humans, respectively.[1] Multiple integrin classes have been implicated in the ability of cells to transform mechanical stimuli such as substrate rigidity, fluid shear, and stretch into intracellular signaling,[2–9] a process termed mechanotransduction. The fibronectin binding integrins $\alpha_v\beta_3$ and $\alpha_5\beta_1$ in particular have attracted considerable interest as drug development targets due to their central roles in wound healing, angiogenesis, and cancer metastasis.[10,11]

Although integrins are acknowledged to play a central role in transmitting and sensing mechanical force, how they do so at a molecular level remains poorly understood. Even the force transmitted by individual integrin heterodimers remains uncertain, with reported values spanning 1 to >100 pN.[12–18] Thus, it is unclear if integrin-based adhesion, and by extension mechanotransduction, reflects a disproportionate contribution by only a few integrins bearing large forces (here, >30 pN), or is instead a collective phenomenon reflecting the cumulative output of many weaker interactions. Conventional techniques are not well-suited to address this problem: both traction force microscopy (TFM) and micropillar array measurements report forces averaged over many integrins, while existing single-molecule techniques such as atomic force microscopy (AFM) and optical tweezers do not recapitulate the complex environment of a cellular adhesion. Recently, we and others have developed fluorescence-based molecular probes that measure force at integrin-based adhesions either by changes in Förster resonance energy transfer (FRET)[12,19–21] or by the force-induced dissociation of DNA duplexes.[22,23] Measurements of this kind have improved the spatial resolution of integrin-based tension measurements to ~50 nm,[19] thereby revealing distinct heterogeneities in local forces within single adhesions. However, to our knowledge the basic question of how forces are apportioned among integrin molecules remains unaddressed.

Results

Single-molecule molecular tension sensor (MTS) measurements quantify loads experienced by individual integrin heterodimers

Here, we used improved molecular tension sensors (MTSs)[12,19] to measure the distribution of forces experienced by individual integrin heterodimers within the adhesion complexes of living cells (Figure 1, see Supplementary Note). To gain further insight into how integrin engagement alters force production, we engineered MTSs presenting either a linear arginine-glycine-aspartate (RGD)-containing peptide derived from fibronectin, here termed MTS_{RGD}, or the complete fibronectin type III 9th and 10th domains ($FNIII_{9-10}$), termed MTS_{FN9-10} (Figure 1a, Figure S1–2, Table S1). MTS_{RGD} provides a minimal binding site for fibronectin-binding integrins (in our system, primarily $\alpha_v\beta_3$ and $\alpha_5\beta_1$), while MTS_{FN9-10} includes a secondary binding site for $\alpha_5\beta_1$ integrin, termed the "synergy site", that is thought to play an essential role in the formation of a force-resistant catch bond between $\alpha_5\beta_1$ integrin and fibronectin.[13,24] To investigate specific contributions of the synergy site, we constructed a third sensor, termed $MTS_{FN9*-10}$, that is identical to MTS_{FN9-10} except that the synergy site motif PHSRN (fibronectin residues 1376-1380) is replaced with SPSDN, the corresponding inactive sequence from $FNIII_8$ (Figure 1a, Figure S3, Table S1).[25,26] Cells did not spread on MTSs lacking an integrin-binding domain (Figure S4).

We first quantified the forces experienced by individual integrin heterodimers by measuring the FRET efficiencies of MTS_{RGD} and MTS_{FN9-10} molecules located underneath human foreskin fibroblasts (HFFs) expressing GFP-paxillin, a focal adhesion marker (Figure 2, Figure S5, see Supporting Information "Calculating single-molecule FRET efficiency"). In this measurement, HFFs adhered to coverslip surfaces on which only 1 in 1000 MTSs were fluorescently labeled, allowing us to measure FRET efficiencies for single sensor molecules (Figure 2a, b, Figure S6). We observed a prominent peak in the FRET distribution at ~80% FRET, similar to the FRET efficiencies measured in the absence of cells (Figure 2c, Figure S7–8), as well as smaller subpopulations with FRET efficiencies of ~60% and ~20%, indicative of probes experiencing appreciable loads (Figure 2c, Figure S9–10). These low-FRET subpopulations were enriched within adhesions (Figure 2c and Figure S10). FRET efficiencies were converted to forces using a FRET-force calibration curve generated from a phenomenological fit to pre-existing calibration data for the elastic spring domain (Figure S9, Figure S11, see Supporting Information "Obtaining theoretical FRET-force calibration curve").[16]

The distributions of single-molecule FRET efficiencies were well described by a linear combination of 3 Gaussian distributions, which could be used in a phenomenological sense to define possible subpopulations of MTSs bearing zero, intermediate, and high loads (Table S2–3, Figure S9–10). For the cell as a whole, this analysis indicated that 60% and 40% of MTS_{RGD} and MTS_{FN9-10} probes were bound to an integrin (Figure 2d, Table S4, see Supporting Information "Estimating unbound fraction of MTSs"). These fractions are consistent with single-molecule tracking measurements suggesting that ~50% of β_3 and β_1 integrins are immobilized outside focal adhesions,[28] though the mechanism of immobilization in the earlier study was unclear. Of the integrin-bound MTS_{RGD} and

MTS_{FN9-10} sensors, we found that approximately 80% and 60% experienced forces of 1–3 pN, 20% and 30% experienced loads of 3–7 pN, and a small population (<10%) bore loads larger than the MTS could measure (>7 pN) (Figure 2d, e, Table S4). This high force subpopulation was enriched within adhesions, with 20% of load-bearing MTS_{RGD} and MTS_{FN9-10} molecules experiencing forces >7 pN (Figure 2d, e, Table S4). The exact magnitude of these higher-force binding interactions is outside the dynamic range of the MTSs used here, but can be addressed using sensors tuned to higher forces.[21,22,29] Importantly, our data account for the large discrepancy in reported force values: while a few integrins potentially exert substantial forces, the majority of ligand-bound integrins for the cell as a whole exert modest forces of 1–7 pN.

To test if the forces transmitted by integrins were dependent on linkage to the actin cytoskeleton, we treated cells with cytochalasin D, an F-actin barbed end-capper. We observed that treating HFFs with 1 μM cytochalasin D led to rapid disassembly of actin stress fibers and focal adhesions at the cell periphery within minutes of drug addition, before the cell shape appreciably changed (Figure S12). The FRET/force distributions of MTS_{RGD} molecules measured under these conditions revealed that low FRET/high force events (>7 pN) were essentially absent while those at lower forces (~3 pN or less) remained (Figure 2e, Table S5). This result suggests that the higher force interactions require connections to a contractile actin cytoskeleton, while minimally tensioned integrin-MTS linkages do not. These data likewise imply that integrins bearing small loads are sufficient for maintaining adhesion at shorter time scales, since cells remained adhered to the coverslip over the course of the experiment (~1 h).

The fibronectin synergy site influences integrin recruitment to adhesions but not overall traction generation

The synergy site on fibronectin, which is present in MTS_{FN9-10} but not MTS_{RGD}, has been implicated in the formation of a force-resistant catch bond with $\alpha_5\beta_1$ integrin.[13,24] It might be expected that the presence of the synergy site would lead to an increase in cellular traction forces due to catch bond formation, $\alpha_5\beta_1$ integrin-dependent myosin II activation,[6,7] or both. However, this did not appear to be the case in our measurements: forces at the single-molecule level measured with MTS_{RGD} and MTS_{FN9-10} were qualitatively similar. Also contrary to expectations, high force (> 7 pN) binding events within adhesions were more prevalent for cells adhering to MTS_{RGD} as compared to MTS_{FN9-10}. This result is remarkable given that both $\alpha_v\beta_3$ and $\alpha_5\beta_1$ integrin have higher binding affinities for the $FNIII_{9-10}$ domains than for linear, RGD-containing peptides,[30] suggesting that the force exerted by integrins is not set solely by their affinity for a given ligand.

To probe the robustness of this result, we next characterized cellular force production at the whole cell level. To do so, we imaged GFP-paxillin expressing HFFs adhering to coverslips functionalized with a continuous field of fluorescently labeled MTSs, which produces a high resolution traction force map (Figure 3a). For each pixel, the measured FRET value was used to define an average force per sensor, for regions within and outside of adhesions. This ensemble measurement combines contributions from both unbound and bound probes, the latter of which may also include probes that are experiencing loads beyond their dynamic

range (see Supporting Information "Ensemble FRET analysis"). The force per sensor measured in this way is thus likely to represent a lower bound for the actual average force per sensor within a given pixel. With this proviso in mind, we found that cells displayed a small but statistically significant higher average force per sensor within adhesions when adhering to MTS_{RGD} vs. MTS_{FN9-10} (2.6 ± 0.09 pN vs. 2.3 ± 0.08 pN; mean $\pm$ S.E.M.) (Figure 3b, c). This trend was consistent with the median force values calculated from single molecule measurements within adhesions (2.6 pN for MTS_{RGD} vs. 1.5 pN for MTS_{FN9-10}). Likewise, the larger difference between forces measured within adhesions relative to outside of adhesions on MTS_{RGD} was also recapitulated (Figure 3b, c, Figure 2d). Thus, single-molecule FRET measurements were representative of force production on the cellular level.

We further separated adhesions based on their location into peripheral and central adhesions (Figure 3b, c, see Supporting Information). We found that while peripheral adhesions displayed higher average force values for cells adhering to MTS_{RGD} than MTS_{FN9-10}, cells adhering to MTS_{FN9-10} generated modest but significantly higher average forces at the small, centrally located adhesions (Figure 3b, c). Separating adhesions based on size alone reproduced this trend: smaller adhesions displayed higher average forces for cells adhering to MTS_{FN9-10} vs. MTS_{RGD} (Figure S13).

To address the possibility that the >7 pN events corresponded to higher forces on MTS_{FN9-10} than on MTS_{RGD} but that it was indistinguishable due to the sensors' dynamic range, we measured total cellular traction using TFM. To our knowledge, a comparison of the cellular traction force outputs as measured by fluorescent force sensors and by more conventional methods such as TFM has not been reported. MTS FRET is measured on glass (GPa stiffness) while TFM requires a deformable substrate (up to 100 kPa), posing a potential limitation in achieving a direct comparison. However, previous studies have shown that cellular traction forces plateau above a rigidity threshold.[31,32] We therefore performed conventional TFM for HFFs adhering to 18 and 47 kPa polyacrylamide gels, both of which were expected to be above this critical rigidity, functionalized with fibronectin, MTS_{RGD}, or MTS_{FN9-10} (Figure 3e, f, Figure S14). For a given ligand, we observed comparable total forces on the 18 kPa *versus* 47 kPa substrate, suggesting we were within or nearing the plateau region of maximal cellular traction production. On the stiffer, 47 kPa surfaces we found that the total forces per cell measured by TFM for fibronectin, MTS_{RGD}, and MTS_{FN9-10} were statistically indistinguishable, and similar in magnitude to those we obtained from MTS FRET maps (Figure 3d, f). Thus, cellular traction forces measured *via* MTS and TFM were comparable under the circumstances studied here, and did not depend strongly on the integrin ligand.

We next examined whether cell engagement with the synergy site might influence adhesion structure or composition. HFFs express both $\alpha_5\beta_1$ and $\alpha_v\beta_3$ integrins (Figure S15), and cells plated on MTS_{FN9-10} displayed $\alpha_5\beta_1$ integrin-rich adhesions both as large plaques at the cell periphery and smaller adhesions under the cell body, a phenotype similar to that of cells plated on full-length fibronectin (Figure 4a, Figure S16). These smaller $\alpha_5\beta_1$ integrin-rich adhesions likely correspond to the centrally located force-producing regions observed with MTS FRET at the ensemble level (Figure 3a, b). In contrast, $\alpha_5\beta_1$ integrin recruitment to peripheral adhesions was largely abrogated in HFFs seeded on coverslips functionalized

with MTS_{RGD}, an observation consistent with prior results[19] and recapitulated for cells adhering to $MTS_{FN9*-10}$ (Figure 4a, Figure S16). Also consistent with prior results, $\alpha_v\beta_3$ integrin localized solely to large adhesions at the cell periphery on all surfaces (Figure 4a, Figure S16).

To further examine the colocalization of integrins with tension, we fixed HFFs plated on MTS_{FN9-10} or $MTS_{FN9*-10}$ and stained for either $\alpha_5\beta_1$ or $\alpha_v\beta_3$ integrin using an Alexa488-tagged secondary antibody (Figure 4b). Consistent with prior work, imaging immediately after fixation allowed us to colocalize low FRET/high force signals with specific proteins detected by immunohistochemistry. Using this approach, we found that both $\alpha_v\beta_3$ and $\alpha_5\beta_1$ integrins colocalized with cellular traction force to a similar, moderate degree for cells adhering to MTS_{FN9-10} (Figure 4b, c). In contrast, $\alpha_v\beta_3$ integrin colocalization with low FRET/high force was significantly higher than that of $\alpha_5\beta_1$ integrin for cells adhering to $MTS_{FN9*-10}$, consistent with results derived with MTS_{RGD} (Figure 4c).[19] Staining HFFs for either paxillin or both $\alpha_v\beta_3$ and $\alpha_5\beta_1$ simultaneously revealed that the 2D correlation with force was higher than that of either integrin alone, and was statistically similar for cells adhering to either MTS_{FN9-10} or $MTS_{FN9*-10}$ (Figure 4c). These results suggest that the presence or absence of the synergy site altered relative $\alpha_v\beta_3$ and $\alpha_5\beta_1$ integrin recruitment, but not total integrin or paxillin recruitment under the conditions examined here.

Engagement with the fibronectin synergy site contributes to robust adhesion in the presence of external load

As discussed above, in our assays integrin engagement with the fibronectin synergy site led to changes in integrin localization, but not to meaningful changes in force output at either the single-integrin or whole-cell levels. However, beyond their role in traction force transmission, integrins play an essential role in ensuring robust adhesion of the cell to the ECM in the face of externally generated loads, for example during embryonic development and wound repair.[33,34] Indeed, previous evidence implicates an interaction between $\alpha_5\beta_1$ integrin and the fibronectin synergy site in robust cell adhesion.[24] To further probe a specific role for this interaction in adhesion, we tested the ability of cells to resist detachment from MTS-coated coverslips using a modification of a previously described centrifugal adhesion assay.[35,36] Briefly, HFFs were seeded onto chambers coated with equimolar concentrations of MTS_{RGD}, MTS_{FN9-10}, or $MTS_{FN9*-10}$ and allowed to attach for 10 min before being centrifuged upside down to apply a sedimentation force (see Supporting Information "Centrifugal adhesion assay"). The fraction of cells that remain attached is an indicator of adhesion strength. Consistent with prior measurements, HFFs seeded on MTS_{FN9-10} functionalized surfaces displayed significantly higher adhesion strength as compared to cells adhering to MTS_{RGD} or $MTS_{FN9*-10}$ (Figure 4d). Thus, in this assay the presence of the fibronectin synergy site led to enhanced cell adhesion in the presence of externally generated mechanical loads.

Average and SEM are calculated from 5 replicates for each condition, drawn from 3 independent experiments. ** $p < 0.001$ using 2-sample t-test.

Conclusions

We used MTSs to directly address how loads are distributed among individual integrin molecules. Previous estimates for the forces experienced by individual integrins range from ~1 to >100 pN.[12,13,15,17,18,20–23,37] Lower estimates have typically come from dividing the traction generated by individual adhesions by the total number of recruited integrins,[18,37] while higher force estimates were derived from integrin-mediated bond rupture measurements[13,38] or the use of fluorescent DNA hairpins of known unfolding force.[21,23] Our data resolve this apparent discrepancy: at least in our model system, a majority of ligand-bound integrins exert modest forces of 1–7 pN, ~10-fold lower than the maximal forces that integrins can potentially bear.[13,15,17,21] However, a smaller population experiencing forces larger than we can measure is enriched within adhesions, consistent with prior measurements indicating that at least a fraction of integrins experience substantial loads. Exactly how forces are distributed within this higher force population is unknown and is an interesting topic for future investigations.

At least in our measurements, the presence of the fibronectin synergy site did not lead to an increase in either overall cellular traction (Figure 3d, f) or loads measured at the single-integrin level (Figure 2d). However, consistent with prior work,[24] interaction with the synergy site increased the ability of cells to resist detachment when exposed to external load (Figure 4d). How exactly this occurs at a molecular level is not clear: resistance to detachment could occur *via* integrin-mediated catch bonds,[13] mechanical reinforcement at the level of single integrins,[38] increased integrin recruitment, or a combination of all of the above. Future studies incorporating changes in MTS density, additional small-molecule based cytoskeletal perturbations, and similar strategies offer a means of differentiating between these and other potential mechanisms of integrin-based mechanosensing.

Our observations support a conceptual distinction between the role of integrins in transmitting cytoskeletally generated traction forces and in mediating robust adhesion of the cell to its substrate. Roughly 50% of MTS_{RGD} and MTS_{FN9-10} molecules outside of defined adhesions experienced measurable loads (Figure 2d), and integrins transmitting approximately 3 pN or less were sufficient to maintain adhesion when the actin cytoskeleton and large adhesions were abrogated by treatment with cytochalasin D (Figure 2e). This integrin population, which would be difficult to observe using other existing techniques, may provide a large pool of engaged but minimally tensioned integrins that can resist cell detachment on short timescales to impart cells and tissues with mechanical integrity.

Methods

Cell culture

HFFs (ATCC, CRL-2091) were cultured in high glucose DMEM (Gibco 21063-045) supplemented with 10% fetal bovine serum (Corning MT35011CV), 1 mM sodium pyruvate (Life Technologies 10010-023), 1x MEM non-essential amino acids (Life Technologies 11140050), and 100 U/ml penicillin/streptomycin (Life Technologies 15140122), herein referred to as normal culture media. Cells were incubated at 37°C with 5% CO_2. Cells stably

expressing GFP-paxillin (GFP at C-terminus) were described previously[18] and cultured identically.

Cloning

Human fibronectin type III repeats 9 and 10 were cloned from FN 108 (Addgene Plasmid #50495) into an existing MTS$_{RGD}$ construct in the pJExpress414 bacterial expression vector[18] (DNA 2.0), replacing the linear RGD sequence and inserting a TEV cleavage site preceding the FN repeats. The existing TAG stop codon for unnatural amino incorporation was mutated using Quikchange mutagenesis (Agilent) to incorporate a reactive cysteine, using the primer 5′-ggcggtgctggcgaattcggtaagtgcggccctggtgg-3′ and its complement. A C-terminal 6xHis tag was used for purification. The HaloTag domain's two native cysteines were previously mutated to serines, without loss of function. The full amino acid sequences of MTSs are provided in Table S1.

Preparation of dye-labeled MTSs

Briefly, sensor proteins were produced using bacterial expression in *E. coli* strain BL21(DE3) and purified using Ni-NTA HisPur resin (Thermo Pierce 88222). Donor and acceptor dye labeling was achieved using a dual-cysteine labeling strategy with maleimide-conjugated Alexa546 and Alexa647 dyes (Life Technologies A10258, A20347) in a 1:2:1.5 protein:Alexa647:Alexa546 ratio. Sensors labeled with both donor and acceptor were separated from MTSs labeled with only the donor or acceptor on a MonoQ PC 1.6/5 column (GE Healthcare 17-0671-01) using an AKTApure FPLC (GE Healthcare) (see Supporting Information "Labeling of MTS constructs").

Flow cell preparation

Perfusion chambers (Grace Biolabs 622103) were adhered to HaloLigand/PEG-functionalized coverslips. Fluorophore labeled or unlabeled MTSs (100 nM) were added to the flow cell and incubated at room temperature for 30 min, washed with PBS twice, and further passivated with 0.2% w/v Pluronic F-127 for 5 minutes. Channels were washed once with PBS before adding freshly trypsinized HFFs in normal culture media and incubated at 37°C with 5% CO_2. Cells were typically allowed to spread for 1 h before imaging, and not imaged for longer than 4 hours after seeding. Chamber inlets and outlets were sealed with tape before imaging to prevent drying out, and cells were imaged at 37°C using an objective heater (Bioptechs).

Single-molecule FRET/force measurements

Single-molecule FRET efficiency data were acquired by constant excitation with 532 nm at 5 frames/sec for 600 frames, with direct acceptor excitation at 635 nm at approximately frame 100 for 10 frames. This strategy was employed to aid in differentiating between MTSs with low FRET values *versus* those lacking a FRET acceptor. Single-molecule FRET calculations were done using custom-made MATLAB code (see Supporting Information "Calculating single-molecule FRET efficiency"). To estimate the fraction of unbound MTS molecules, we fit the cumulative distributions of single-molecule FRET efficiencies to a sum of Gaussians. The highest FRET efficiency population was similar to the no-load FRET

efficiency measured in the absence of cells (Table S2, Figure S7). This subpopulation was therefore assigned as the MTSs under zero load (*i.e.* not bound to an integrin) (see Supporting Information "Estimating unbound fraction of MTSs"). The FRET vs. force response of the (GPGGA)$_8$ linker used here was previously reported by Grashoff *et al.*[16] We adjusted this calibration to account for the biophysical and photophysical properties of the MTSs used here (see Supporting Information "Obtaining theoretical FRET-force calibration curve").

Supplementary Material

Refer to Web version on PubMed Central for supplementary material.

Acknowledgments

References

1. Hynes RO. Integrins: Bidirectional, Allosteric Signaling Machines. Cell. 2002; 110:673–687. [PubMed: 12297042]

2. Engler AJ, Sen S, Sweeney HL, Discher DE. Matrix Elasticity Directs Stem Cell Lineage Specification. Cell. 2006; 126:677–689. [PubMed: 16923388]

3. Tzima E, Irani-Tehrani M, Kiosses WB, Dejana E, Schultz Da, Engelhardt B, Cao G, DeLisser H, Schwartz MA. A Mechanosensory Complex That Mediates the Endothelial Cell Response to Fluid Shear Stress. Nature. 2005; 437:426–431. [PubMed: 16163360]

4. Ross TD, Coon BG, Yun S, Baeyens N, Tanaka K, Ouyang M, Schwartz Ma. Integrins in Mechanotransduction. Curr Opin Cell Biol. 2013; 25:613–618. [PubMed: 23797029]

5. Puklin-Faucher E, Sheetz MP. The Mechanical Integrin Cycle. J Cell Sci. 2009; 122:179–186. [PubMed: 19118210]

6. Schiller HB, Hermann MR, Polleux J, Vignaud T, Zanivan S, Friedel CC, Sun Z, Raducanu A, Gottschalk KE, Théry M, Mann M, Fässler R. β1- and αv-Class Integrins Cooperate to Regulate Myosin II during Rigidity Sensing of Fibronectin-Based Microenvironments. Nat Cell Biol. 2013; 15:625–636. [PubMed: 23708002]

7. Danen EHJ, Sonneveld P, Brakebusch C, Fässler R, Sonnenberg A. The Fibronectin-Binding Integrins α5β1 and αvβ3 Differentially Modulate RhoA-GTP Loading, Organization of Cell Matrix Adhesions, and Fibronectin Fibrillogenesis. J Cell Biol. 2002; 159:1071–1086. [PubMed: 12486108]

8. Truong H, Danen EHJ. Integrin Switching Modulates Adhesion Dynamics and Cell Migration. Cell Adh Migr. 2009; 3:179–181. [PubMed: 19287215]

9. Elosegui-Artola A, Bazellières E, Allen MD, Andreu I, Oria R, Sunyer R, Gomm JJ, Marshall JF, Jones JL, Trepat X, Roca-Cusachs P. Rigidity Sensing and Adaptation through Regulation of Integrin Types. Nat Mater. 2014; 13:631–637. [PubMed: 24793358]

10. Cox D, Brennan M, Moran N. Integrins as Therapeutic Targets: Lessons and Opportunities. Nat Rev Drug Discov. 2010; 9:804–820. [PubMed: 20885411]

11. Schaffner F, Ray AM, Dontenwill M. Integrin α5β1, the Fibronectin Receptor, as a Pertinent Therapeutic Target in Solid Tumors. Cancers (Basel). 2013; 5:27–47. [PubMed: 24216697]

12. Morimatsu M, Mekhdjian AH, Adhikari AS, Dunn AR. Molecular Tension Sensors Report Forces Generated by Single Integrin Molecules in Living Cells. Nano Lett. 2013; 13:3985–3989. [PubMed: 23859772]

13. Kong F, García AJ, Mould AP, Humphries MJ, Zhu C. Demonstration of Catch Bonds between an Integrin and Its Ligand. J Cell Biol. 2009; 185:1275–1284. [PubMed: 19564406]

14. Jiang G, Giannone G, Critchley DR, Fukumoto E, Sheetz MP. Two-Piconewton Slip Bond between Fibronectin and the Cytoskeleton Depends on Talin. Nature. 2003; 424:334–337. [PubMed: 12867986]

15. Li F, Redick SD, Erickson HP, Moy VT. Force Measurements of the α5β1 Integrin-Fibronectin Interaction. Biophys J. 2003; 84:1252–1262. [PubMed: 12547805]

16. Grashoff C, Hoffman BD, Brenner MD, Zhou R, Parsons M, Yang MT, McLean MA, Sligar SG, Chen CS, Ha T, Schwartz MA. Measuring Mechanical Tension across Vinculin Reveals Regulation of Focal Adhesion Dynamics. Nature. 2010; 466:263–266. [PubMed: 20613844]

17. Thoumine O, Kocian P, Kottelat A, Meister JJ. Short-Term Binding of Fibroblasts to Fibronectin: Optical Tweezers Experiments and Probabilistic Analysis. Eur Biophys J. 2000; 29:398–408. [PubMed: 11081401]

18. Balaban NQ, Schwarz US, Riveline D, Goichberg P, Tzur G, Sabanay I, Mahalu D, Safran S, Bershadsky A, Addadi L, Geiger B. Force and Focal Adhesion Assembly: A Close Relationship Studied Using Elastic Micropatterned Substrates. Nat Cell Biol. 2001; 3:466–472. [PubMed: 11331874]

19. Morimatsu M, Mekhdjian AH, Chang AC, Tan SJ, Dunn AR. Visualizing the Interior Architecture of Focal Adhesions with High-Resolution Traction Maps. Nano Lett. 2015; 15:2220–2228. [PubMed: 25730141]

20. Liu Y, Yehl K, Narui Y, Salaita K. Tension Sensing Nanoparticles for Mechano-Imaging at the Living/nonliving Interface. J Am Chem Soc. 2013; 135:5320–5323. [PubMed: 23495954]

21. Galior K, Liu Y, Yehl K, Vivek S, Salaita K. Titin-Based Nanoparticle Tension Sensors Map High-Magnitude Integrin Forces within Focal Adhesions. Nano Lett. 2016; 16:341–348. [PubMed: 26598972]

22. Blakely BL, Dumelin CE, Trappmann B, McGregor LM, Choi CK, Anthony PC, Duesterberg VK, Baker BM, Block SM, Liu DR, Chen CS. A DNA-Based Molecular Probe for Optically Reporting Cellular Traction Forces. Nat Methods. 2014; 11:1229–1232. [PubMed: 25306545]

23. Wang X, Ha T. Defining Single Molecular Forces Required to Activate Integrin and Notch Signaling. Science. 2013; 340:991–994. [PubMed: 23704575]

24. Friedland JC, Lee MH, Boettiger D. Mechanically Activated Integrin Switch Controls α5β1 Function. Science. 2009; 323:642–644. [PubMed: 19179533]

25. Danen EHJ, Aota S-i, van Kraats AA, Yamada KM, Ruiter DJ, van Muijen GNP. Requirement for the Synergy Site for Cell Adhesion to Fibronectin Depends on the Activation State of Integrin α5β1. J Biol Chem. 1995; 270:21612–21618. [PubMed: 7545166]

26. Mould A, Askari J, Humphries MJ. Molecular Basis of Ligand Recognition by Integrin α5β1. I. Specificity of Ligand Binding Is Determined by Amino Acid Sequences in the Second and Third NH2-Terminal Repeats of the Alpha Subunit. J Biol Chem. 2000; 275:20324–20336. [PubMed: 10764748]

27. Brenner MD, Zhou R, Conway DE, Lanzano L, Gratton E, Schwartz MA, Ha T. Spider Silk Peptide Is a Compact, Linear Nano-Spring Ideal for Intracellular Tension Sensing. Nano Lett. 2016; 16:2096–2102. [PubMed: 26824190]

28. Rossier O, Octeau V, Sibarita JB, Leduc C, Tessier B, Nair D, Gatterdam V, Destaing O, Albigès-Rizo C, Tampé R, Cognet L, Choquet D, Lounis B, Giannone G. Integrins β1 and β3 Exhibit Distinct Dynamic Nanoscale Organizations inside Focal Adhesions. Nat Cell Biol. 2012; 14:1057–1067. [PubMed: 23023225]

29. Austen K, Ringer P, Mehlich A, Chrostek-Grashoff A, Kluger C, Klingner C, Sabass B, Zent R, Rief M, Grashoff C. Extracellular Rigidity Sensing by Talin Isoform-Specific Mechanical Linkages. Nat Cell Biol. 2015; 17:1597–1606. [PubMed: 26523364]

30. Pfaff M, Tangemann K, Müller B, Gurrath M, Müller G, Kessler H, Timpl R, Engel J. Selective Recognition of Cyclic RGD Peptides of NMR Defined Conformation by αIIbβ3, αvβ3, and α5β1 Integrins. J Biol Chem. 1994; 269:20233–20238. [PubMed: 8051114]

31. Ghibaudo M, Saez A, Trichet L, Xayaphoummine A, Browaeys J, Silberzan P, Buguin A, Ladoux B. Traction Forces and Rigidity Sensing Regulate Cell Functions. Soft Matter. 2008; 4:1836.

32. Elosegui-Artola A, Oria R, Chen Y, Kosmalska A, Pérez-González C, Castro N, Zhu C, Trepat X, Roca-Cusachs P. Mechanical Regulation of a Molecular Clutch Defines Force Transmission and Transduction in Response to Matrix Rigidity. Nat Cell Biol. 2016; 18:540–548. [PubMed: 27065098]

33. Bökel C, Brown NH. Integrins in Development: Moving On, Responding To, and Sticking to the Extracellular Matrix. Dev Cell. 2002; 3:311–321. [PubMed: 12361595]

34. Martin P. Wound Healing--Aiming for Perfect Skin Regeneration. Science. 1997; 276:75–81. [PubMed: 9082989]

35. McClay, DR., Hertzler, PL. Current Protocols in Cell Biology. John Wiley & Sons, Inc; Hoboken, NJ, USA: 2001. Quantitative Measurement of Cell Adhesion Using Centrifugal Force; p. 9.2.1-9.2.10.

36. Reyes CD, García AJ. A Centrifugation Cell Adhesion Assay for High-Throughput Screening of Biomaterial Surfaces. J Biomed Mater Res A. 2003; 67:328–333. [PubMed: 14517892]

37. Roca-Cusachs P, Gauthier NC, del Rio A, Sheetz MP. Clustering of α5β1 Integrins Determines Adhesion Strength Whereas αvβ3 and Talin Enable Mechanotransduction. Proc Natl Acad Sci. 2009; 106:16245–16250. [PubMed: 19805288]

38. Kong F, Li Z, Parks WM, Dumbauld DW, García AJ, Mould AP, Humphries MJ, Zhu C. Cyclic Mechanical Reinforcement of Integrin-Ligand Interactions. Mol Cell. 2013; 49:1060–1068. [PubMed: 23416109]
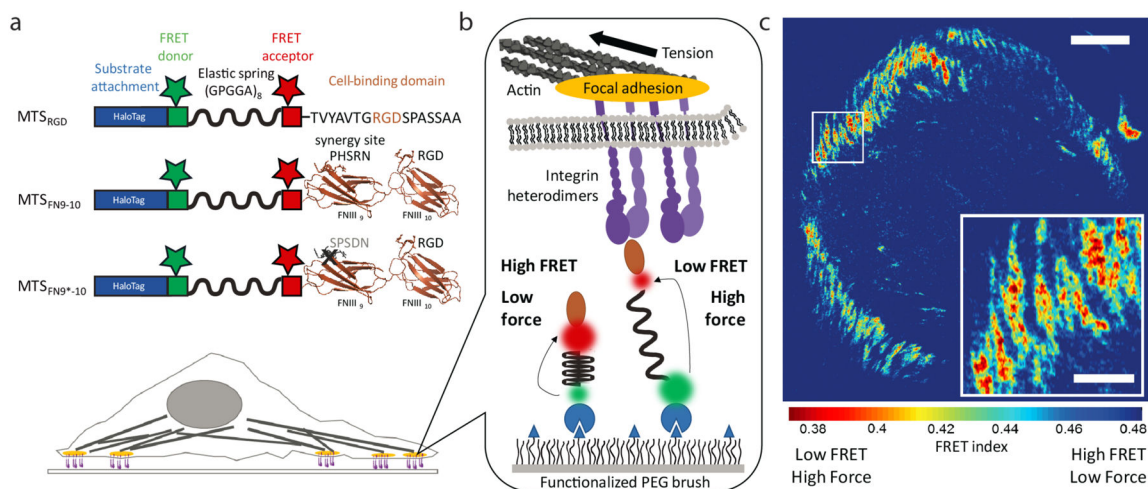
Figure 1. Molecular tension sensors
a) MTSs contain an N-terminal, cysteine-free HaloTag domain, two reactive cysteines for attachment of a FRET donor and acceptor, an elastic spring domain derived from spider silk, and a C-terminal integrin binding ligand: a linear RGD peptide derived from fibronectin (MTS_{RGD}), the $FNIII_{9-10}$ domains (MTS_{FN9-10}), or the $FNIII_{9-10}$ domains with an inactive synergy site ($MTS_{FN9*-10}$). Image of the $FNIII_{9-10}$ domains based on protein structure 1FNF and rendered using PyMOL. **b)** Sensors attach covalently to a PEG-functionalized glass coverslip *via* the HaloTag domain. Cell-generated force pulls the FRET donor and acceptor apart, causing a decrease in FRET efficiency. The force/FRET relation for the spring domain has been previously calibrated,[16,27] allowing us to relate FRET efficiency to force (see Supporting Information and Figure S9). **c)** When fluorescently labeled sensors are attached to a coverslip at high density and cells are allowed to spread on the surface, imaging the FRET donor and acceptor fluorescence yields a high-resolution traction map. FRET index, defined here as the ratio of acceptor intensity over summed donor and acceptor intensity, is used as a relative measure for FRET efficiency: a low FRET index indicates high force and a high FRET index indicates low force. FRET index map of an HFF seeded on MTS_{FN9-10}. Scale bar = 15 μm. Inset scale bar = 5 μm.
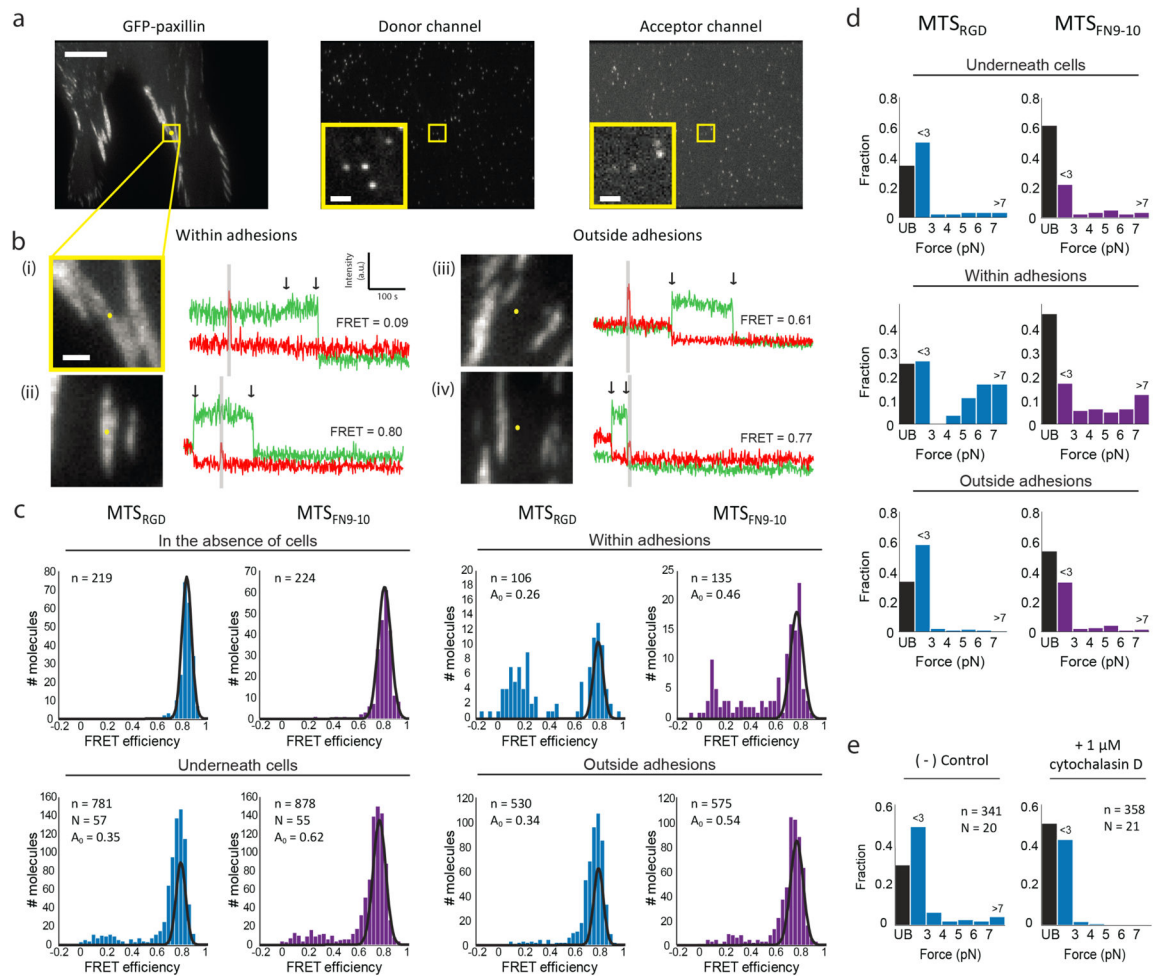
Figure 2. MTSs measure the forces exerted by single integrins within adhesions in living cells
a) Representative images of the GFP, donor, and acceptor channels for a GFP-paxillin expressing HFF spread on a coverslip prepared with a single-molecule density of labeled MTS_{FN9-10}. Scale bar = 10 μm. Yellow squares indicate a region of interest (insets plus **bi**). Inset scale bar = 1 μm. **b)** Four GFP-paxillin images with the tracked MTS_{FN9-10} location marked as a yellow dot. The corresponding single molecule fluorescence traces are shown to the right. The first arrow indicates acceptor (red) bleach and donor (green) recovery; the second arrow indicates donor bleach. Gray zones correspond to direct excitation of the FRET acceptor. Excitation at 635 nm increases the fluorescence background, which results in a small increase in counts in the acceptor emission channel in traces *ii* and *iv*. Examples traces include MTS_{FN9-10} molecules within adhesions (i, ii) and outside adhesions (iii, iv), with low (i, iii) and high (ii, iv) FRET values. **c)** FRET efficiency histograms for MTS_{RGD} (blue) and MTS_{FN9-10} (purple) measured in the absence of cells, underneath cells, within adhesions, and outside adhesions. Black curves represent single-Gaussian fits to the no-load distributions (in the absence of cells), and to A_0, the proportion of the distribution corresponding to unbound sensors obtained from a 3 Gaussian fit to the data in the presence of cells (see Supporting Information). **d)** FRET values from **c** converted to forces. Black bar (UB, unbound) indicates the fraction of MTS molecules that are assigned as not bound to an

integrin. **e)** FRET efficiency values converted to forces for MTS_{RGD} molecules measured underneath cells before (left) and after (right) treatment with 1 μM cytochalasin D. $n =$ number of molecules, $N =$ number of cells.
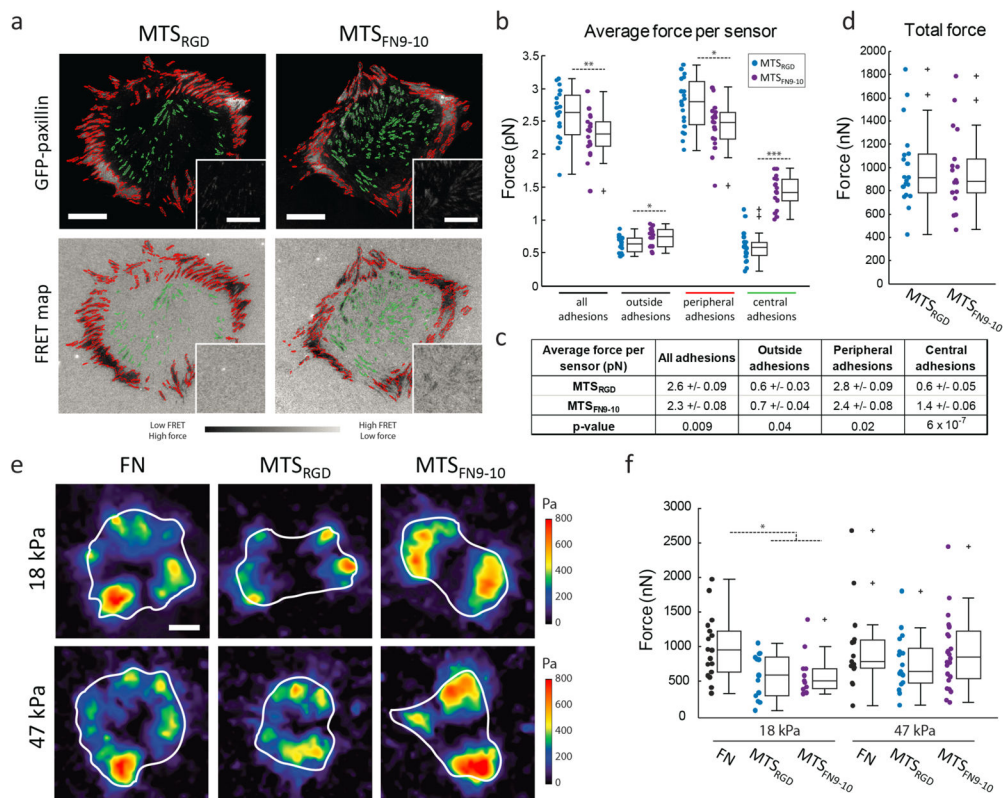
Figure 3. MTS measurements and TFM report comparable total cellular traction forces
a) Representative GFP-paxillin images and corresponding FRET maps for live, transfected HFFs seeded on MTS$_{RGD}$- and MTS$_{FN9-10}$-functionalized glass coverslips. Peripheral adhesions (red) and central adhesions (green) were segmented based on the GFP signal and the resulting mask was applied to the FRET channel. Scale bar = 20 μm, inset scale bar = 10 μm. **b)** Average force values per sensor for all, peripheral, and central adhesions, and outside of adhesions on MTS$_{RGD}$ (blue, $n = 19$ cells) and MTS$_{FN9-10}$ (purple, $n = 18$ cells). **c)** Table of average forces per sensor (mean +/− S.E.M.) for all subsets of adhesions, with p-values determined *via* the two-sided Wilcoxon rank sum test. **d)** Total forces per cell as measured with MTS FRET on glass. **e)** Representative traction maps for GFP-paxillin expressing HFFs (white = cell outline) plated on 18 kPa (top) or 47 Pa (bottom) polyacrylamide gels coated with full-length fibronectin (FN), MTS$_{RGD}$, or MTS$_{FN9-10}$. Scale bar = 20 μm. **f)** Quantification of total force per cell obtained using TFM. Number of cells per condition from left to right is 18, 14, 11, 15, 17, 24. *p < 0.05, **p < 0.01, ***p < 1 × 10^{-6} using two-sided Wilcoxon rank sum test.
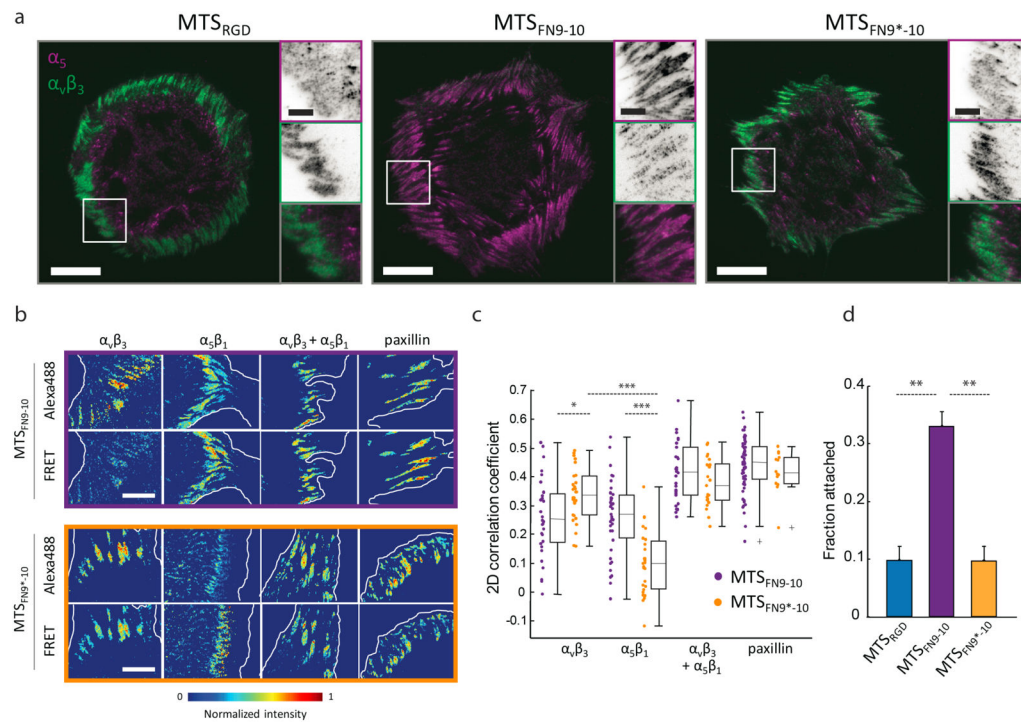
Figure 4. The fibronectin synergy site controls integrin recruitment to force-bearing adhesions
a) HFFs plated on MTS_{RGD}, MTS_{FN9-10}, or $MTS_{FN9*-10}$ and stained for α_5 integrin (magenta) and $\alpha_v\beta_3$ integrin (green). Scale bar = 20 μm, inset scale bar = 5 μm. **b)** Wild-type HFFs were seeded on MTS_{FN9-10} or $MTS_{FN9*-10}$ and fixed and stained for $\alpha_v\beta_3$ integrin, $\alpha_5\beta_1$ integrin, both integrins together, or paxillin using an Alexa488-labeled secondary antibody, and imaged concurrently with MTS FRET (see Supporting Information). Scale bar = 10 μm. **c)** 2D Pearson correlation coefficients between FRET and Alexa488 intensity values for cells adhering to MTS_{FN9-10} and $MTS_{FN9*-10}$. Each data point corresponds to one field of view, where a field corresponds to one distinct cell ($n = 32, 29, 30, 53$ cells for MTS_{FN9-10}, $n = 30, 27, 21$, and 14 for $MTS_{FN9*-10}$, from left to right). *p < 0.05, ***p < 1×10^{-5} using two-sided Wilcoxon rank sum test. d) Cells were seeded on MTS-coated surfaces, inverted, and centrifuged to apply external detachment forces. Remaining cells were counted after centrifugation to calculate the fraction of cells still attached.